Title
Individual IKs channels at the surface of mammalian cells contain two KCNE1 accessory subunits.

Journal
Proceedings of the National Academy of Sciences of USA, 111(14)

Authors
Plant, Leigh
Xiong, Dazhi
Dai, Hui
et al.

Publication Date
2014-04-08

DOI
10.1073/pnas.1323548111

Peer reviewed

Individual I_{Ks} channels at the surface of mammalian cells contain two KCNE1 accessory subunits

Leigh D. Plant[1], Dazhi Xiong[1], Hui Dai, and Steve A. N. Goldstein[2]

Department of Biochemistry, Brandeis University, Waltham, MA, 02453

Edited by Richard W. Aldrich, The University of Texas at Austin, Austin, TX, and approved February 4, 2014 (received for review December 17, 2013)

KCNE1 (E1) β-subunits assemble with KCNQ1 (Q1) voltage-gated K^+ channel α-subunits to form I_{Kslow} (I_{Ks}) channels in the heart and ear. The number of E1 subunits in I_{Ks} channels has been an issue of ongoing debate. Here, we use single-molecule spectroscopy to demonstrate that surface I_{Ks} channels with human subunits contain two E1 and four Q1 subunits. This stoichiometry does not vary. Thus, I_{Ks} channels in cells with elevated levels of E1 carry no more than two E1 subunits. Cells with low levels of E1 produce I_{Ks} channels with two E1 subunits and Q1 channels with no E1 subunits—channels with one E1 do not appear to form or are restricted from surface expression. The plethora of models of cardiac function, transgenic animals, and drug screens based on variable E1 stoichiometry do not reflect physiology.

minK | LQTS | single-particle fluorimetry | K_V7.1 | K_VLQT1

Voltage-gated potassium (K_V) channels include four α-subunits that form a single, central ion conduction pathway with four peripheral voltage sensors (1–3). Incorporation of accessory β-subunits modifies the function of K_V channels to suit the diverse requirements of different tissues. KCNE genes encode minK-related peptides (MiRPs) (4–6), β-subunits with a single transmembrane span that assemble with a wide array of K_V α-subunits (7, 8) to control surface expression, voltage dependence, and kinetics of gating transitions, unitary conductance, ion selectivity, and pharmacology of the resultant channel complexes (4, 9–15). I_{Kslow} (I_{Ks}) channels in the heart and inner ear are formed by the α-subunit encoded by KCNQ1 (called Q1, K_VLQT1, K_V7.1, or KCNQ1) and the β-subunit encoded by KCNE1 (called E1, mink, or KCNE1) (16, 17). Inherited mutations in Q1 and E1 are associated with cardiac arrhythmia and deafness.

The number of E1 subunits in I_{Ks} channels has been a longstanding matter of disagreement. We first argued for two E1 subunits per channel based on the suppression of current by an E1 mutant (18). Subsequently, we reached the same conclusion by determining the total number of channels using radiolabeled charybdotoxin (CTX), a scorpion toxin that blocks channels when one molecule binds in the external conduction pore vestibule, and an antibody-based luminescence assay to tally E1 subunits (19). Morin and Kobertz (20) used iterative chemical linkage between CTX in the pore and E1, and they also assigned two accessory subunits to >95% of I_{Ks} channels without gathering evidence for variation in subunit valence. Furthermore, when we formed I_{Ks} channels from separate E1 and Q1 subunits and compared them with channels enforced via genetic encoding to contain two or four E1 subunits (19), we observed the natural I_{Ks} channels to have the same gating attributes, small-molecule pharmacology, and CTX on and off rates (a reflection of pore vestibule structure) as channels encoded with two E1 subunits but not those with four. These findings support the conclusion that two E1 subunits are necessary, sufficient, and the normal number in I_{Ks} channels.

In contrast, others have argued that I_{Ks} channels have variable stoichiometry with one to four E1 subunits, or even more (21–24). Recently, Nakajo et al. (25) applied single-particle spectroscopy to the question; this powerful "gold-standard" tool has been a valuable strategy to assess the subunit composition of ion channels (26–28) and should be expected to improve on prior investigations conducted on populations of I_{Ks} channels and subject, therefore, to the simplifying assumptions that attend macroscopic studies (29). Nakajo et al. (25) reported a variable number of E1 subunits, from one to four, in I_{Ks} channels studied in *Xenopus laevis* oocytes. The impact of this result has been striking because it has engendered new models of cardiac physiology, altered models of I_{Ks} channel biosynthesis and function, stimulated the use of transgenic animals artificially enforced to express I_{Ks} channels with four E1 subunits (by expression of a fused E1–Q1 subunit), and prompted cardiac drug design based on the assumption that I_{Ks} channels can form with one E1 subunit (23, 30–32).

We were concerned that the conclusions of Nakajo et al. (25) were in error because they appraised only a limited fraction of particles that were immobile in the oocyte membrane; counted E1 and Q1 asynchronously rather than simultaneously (increasing the risk that particles moved into or out of the field of view); and studied Q1 and E1 appended not only with the fluorescent proteins (FP) required to count subunits by photobleaching but also with a common trafficking motif that suppressed channel mobility by interacting with an overexpressed anchoring protein, thereby risking nonnatural aggregation of subunits.

Here, to resolve mobility problems and obviate the need for modification of subunits with targeting motifs, we describe and perform single-fluorescent-particle photobleaching at the surface of live mammalian cells, demonstrating three spectroscopic counting approaches: standard, asynchronous subunit counting; simultaneous, two-color subunit counting; and toxin-directed, simultaneous, two-color photobleaching. To analyze the data, we use two

Significance

I_{Kslow} (I_{Ks}) channels allow heartbeats and hearing. The channels contain two types of subunits: Q1 and E1. Both are required. While four Q1 subunits are known to form the pore, the number of E1 subunits has been controversial for over a decade. The answer is critical to understanding cardiac function, diseases, including life-threatening arrhythmias, and for drug development. Here, we describe an improved method to study the composition and surface density of single I_{Ks} channels—simultaneous, two-color, subunit counting for channels on the surface of live mammalian cells. We show that I_{Ks} channels contain two E1 subunits and four Q1 subunits. This subunit ratio does not vary even when levels of E1 are raised or lowered 10-fold as found in tissues.

Author contributions: L.D.P. and S.A.N.G. designed research; L.D.P., D.X., and H.D. performed research; L.D.P., D.X., and S.A.N.G. analyzed data; and L.D.P., D.X., and S.A.N.G. wrote the paper.

The authors declare no conflict of interest.

This article is a PNAS Direct Submission.

Freely available online through the PNAS open access option.

See Commentary on page 5065.

[1]L.D.P. and D.X. contributed equally to this work.

[2]To whom correspondence should be addressed. E-mail: goldstein@brandeis.edu.

This article contains supporting information online at www.pnas.org/lookup/suppl/doi:10.1073/pnas.1323548111/-/DCSupplemental.

statistical approaches—one to assess the degree of colocalization of objects in dual-color images (33) and the other to infer stoichiometry from single-molecule photobleaching (34). These methods also allow determination of the surface density of assemblies of defined subunit composition and are therefore useful to assess the formation and life cycle of membrane protein complexes.

We report that single I_{Ks} channels at the surface of mammalian cells contain two E1 subunits—no more and no less. This finding refutes the single-particle studies of Nakajo et al. (25) in oocytes and macroscopic studies (21–24, 30–32), arguing that forcing cells to express excess E1 produces I_{Ks} channels containing more than two E1 subunits and that low levels of E1 yields I_{Ks} channels with less than two E1 subunits. Not once did we observe an I_{Ks} channel with three or four E1 subunits. Moreover, simultaneous, two-color subunit counting revealed that low amounts of E1 relative to Q1 [ratios like those reported in human cardiac ventricle (35, 36)] produced two types of channels on the cell surface: I_{Ks} channels (with two E1 subunits) and Q1 channels (with no E1 subunits). Finally, E1 was shown to increase in I_{Ks} channel surface expression threefold, as we predicted based on assessment of I_{Ks} channel unitary conductance (11), whereas few E1 subunits were on the surface outside of I_{Ks} channels, even when E1 was expressed alone. This finding indicates that E1 does not travel to the surface readily on its own, that two E1 subunits facilitate I_{Ks} channel trafficking to the surface (or enhance surface residence time compared with Q1 channels), and that I_{Ks} channels with only one E1 subunit do not form, do not reach the surface, or are rapidly recycled.

Results

FP Tags Do Not Alter the Biophysical Properties of I_{Ks} or Q1 Channels. Single-fluorescent-particle photobleaching employs modification of subunits by genetic encoding so that each subunit carries one FP. To confirm that FPs did not alter the electrophysiological attributes of channels, we expressed the wild-type and FP-tagged human E1 and Q1 subunits in Chinese hamster ovary (CHO) cells (Fig. 1 and *SI Appendix*, Table S1) using described methods (27). CHO cells are valuable for studies of I_{Ks} channels (11), especially compared with *Xenopus* oocytes that express amphibian KCNQ1 and KCNE family subunits (16, 37–39), because they pass such low natural levels of potassium current (37). Thus, currents evoked in cells expressing Q1 channels heterologously (formed by Q1 in the absence of added E1) during a 2-s step to 60 mV showed a rise time to half-maximal current (τ_{act}) of 29 ± 20 ms, a half-maximal activation voltage ($V_{1/2}$) of −15.4 ± 1.5 mV, a tail current "hook" during deactivation at the holding voltage (indicative of prior inactivation), and a half-deactivation time constant (τ_{deact}) of 232 ± 12 ms (n = 5) (Fig. 1*A*). As expected (11), coexpression of equal amounts of E1 with Q1 produced isochronal I_{Ks} currents that were ∼10-fold larger, did not saturate during a 2-s step to 60 mV, showed a slower rise τ_{act} of 508 ± 41 ms, an ∼45-mV shift in $V_{1/2}$ to 33 ± 2.5 mV, no hook during deactivation, and a slowed τ_{deact} of 606 ± 42 ms (n = 5) (Fig. 1*A*). Channels formed when one or both subunits carried FP tags produced currents like those observed with wild-type E1 and Q1 subunits (Fig. 1*B* and *SI Appendix*, Table S1). This result was the case with all constructs produced for these studies: E1 modified to carry the monomeric teal FP mTFP1 (E1–TFP), the monomeric yellow FP mVenus (E1–VFP), and the monomeric red FP TagRFP-T (E1–RFP) and Q1 modified to carry TagRFP-T (Q1–RFP) (*Materials and Methods*).

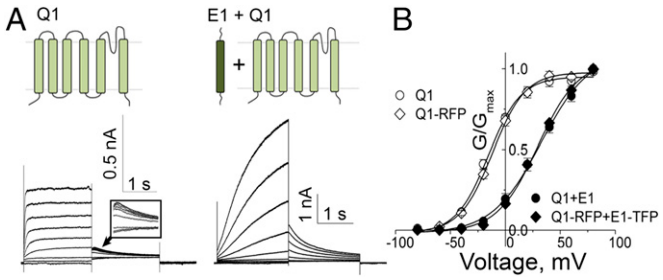

Fig. 1. Biophysical properties of channels. Untagged or RFP-tagged Q1 was expressed alone, or with E1 subunits tagged as indicated, in CHO cells and studied by voltage-clamp in whole-cell mode. Currents were evoked and studied as described in *Materials and Methods*. E1 slows the kinetics of Q1, augments the current magnitude, and depolarizes the $V_{1/2}$ of activation. Data are means ± SEM for five cells studied in each group. Biophysical parameters are summarized in *SI Appendix*, Table S1. (*A*) A cartoon of Q1 and E1 subunits. Representative families of ionic currents in cells expressing Q1 alone or E1 + Q1 are shown. (*Inset*) A magnified view of the tail current hook. (*B*) Normalized *G-V* relationships for Q1 (○), Q1–RFP (◇), untagged Q1 and E1 (●), and Q1–RFP and E1–TFP (◆).

Classical (Asynchronous) Photobleaching Shows No More than Two E1 Subunits in Each Complex. Photobleaching was developed to determine the subunit stoichiometry of membrane protein complexes in *Escherichia coli* (40) and later was used to study ion channels heterologously expressed in *Xenopus* oocytes (26, 41, 42). We recently extended this approach to study the composition of ion channels in mammalian cells to count pore-forming subunits and to monitor modification of channels by small ubiquitin-like modifier proteins (27, 28, 43). Others have also described benefits of performing photobleaching studies in mammalian cells (44, 45). Thus, the CHO cells used here to study human I_{Ks} channel subunits show little confounding particle mobility at room temperature.

E1 encoded to carry each FP was expressed with Q1, and total internal reflection fluorescence microscopy (TIRFM) was used to identify and excite single fluorescent particles at the CHO cell surface (Fig. 2*A*). The number of fluorophores in each particle was determined by continuous photobleaching and counting of stepwise decreases in fluorescence intensity (Fig. 2*B*). Here, particles were formed with equal amounts of cDNA for Q1 and E1 tagged with one of the FPs. Two stepwise decreases in fluorescence were seen in 88%, 80%, and 81% of particles with E1–TFP, E1–VFP, and E1–RFP, respectively, with residual particles showing one step (Fig. 2*C* and *SI Appendix*, Table S2). Arguing against more than two E1 subunits in I_{Ks} channels, no particle showed more than two steps. To support the conclusion from electrophysiology (Fig. 1 and *SI Appendix*, Table S1) that bona fide I_{Ks} channels were being produced for study by TIRFM, surface channels formed by Q1–RFP and E1 were also evaluated. As expected for a tetrameric channel (28, 41), fluorescent particles showed up to four bleaching steps with fractional magnitudes for four, three, two, and one steps of 34%, 37%, 21%, and 8%, respectively (Fig. 2 *D* and *E* and *SI Appendix*, Table S2). No fluorescent particles were observed in cells expressing subunits that did not carry a FP.

Statistics of Single-Particle Photobleaching. Photobleaching events are missed due to prebleaching, quantum efficiency of the fluorophore, and time resolution of the system (27, 41). To evaluate the risk that we were incorrectly estimating the number of E1 subunits in I_{Ks} channels, we applied the recently published statistical approach of Hines (34) for inferring subunit stoichiometry from photobleaching studies. Predicated upon a binomial distribution of FP photobleaching steps in multimeric assemblies, and iterative comparison of the data to up to 10,000 possible outcomes for combinations of the number of observations and the probability of observing each possible fluorescence event (θ), the estimated likelihood that our classical counting data accurately represent two E1 subunits in each I_{Ks} complex is >0.99 (*SI Appendix*, Table S2). Similarly, the observed frequencies for one bleaching step were those expected by the model for complexes with

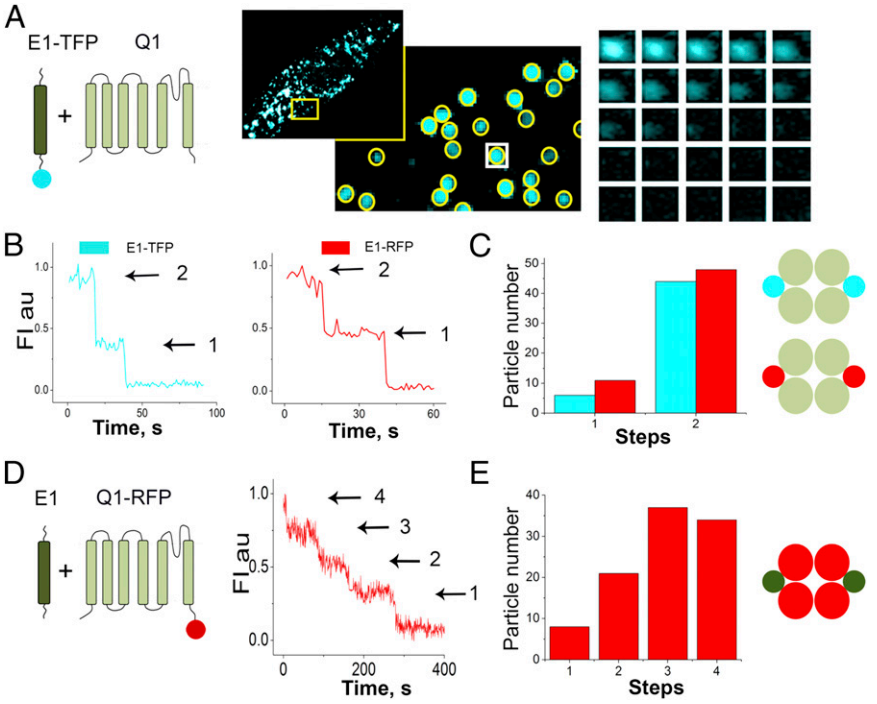

Fig. 2. Sequential photobleaching of FP-tagged E1 or Q1 subunits. E1–TFP or E1–RFP was expressed with untagged Q1 in CHO cells and studied by TIRF and single-particle photobleaching as described in *Materials and Methods*. Data are means ± SEM for five cells studied in each group. Photobleaching parameters are summarized in *SI Appendix*, Tables S2–S4. (*A*, *Left*) Cartoon of E1–TFP and Q1 subunits showing TFP on the E1 C terminus. (*Center*) TIRFM image of a CHO cell expressing E1–TFP + Q1 subunits with an enlargement of the yellow box to show representative cell surface fluorescent particles that were studied for photobleaching (yellow circles). (*Right*) Montage of photobleaching time course of a single fluorescent particle (shown in white box in *Center* panel), during continuous excitation to bleach the fluorophores. Every fifth frame is shown. (*B*) Photobleaching time course for representative particles shows two stepwise changes in fluorescence intensity for cells expressing E1–TFP + Q1 (*Left*; teal) or E1–RFP + Q1 (*Right*; red). (*C Left*) Histogram of bleaching steps for cells expressing E1–TFP + Q1 (teal bars) or E1–RFP + Q1 (red bars). No particles had more than two bleaching steps. (*Right*) Cartoon to indicate that the data analyzed by the approach of Hines estimate two E1 subunits in surface particles formed with E1–TFP or E1–RFP, with an estimated confidence of >0.9 (*SI Appendix*, Table S2); here, the particles are assumed to have four Q1 subunits. (*D*, *Left*) Cartoon of E1 and Q1–RFP subunits showing RFP on the Q1 C terminus. (*Right*) Time course for photobleaching representative fluorescent spots from CHO cells expressing Q1–RFP + E1, showing four stepwise decreases in fluorescence intensity. (*E*, *Left*) Histogram of bleaching steps for cells expressing E1 + Q1–RFP. No particles with more than four bleaching steps were observed. (*Right*) Cartoon to indicate that the data analyzed by the approach of Hines estimates four Q1 subunits in surface particles formed with E1 + Q1–RFP with an estimated confidence of 0.74 (*SI Appendix*, Table S2); here, the particles are assumed to have two E1 subunits.

two E1 subunits (we collected ∼10-fold more observations than required to reach an estimated confidence level of >0.99).

Simultaneous, Two-Color, Single-Particle Photobleaching. Assessing a single FP subunit leaves uncertain whether the complexes under study contain all subunits of interest. Moreover, the extended periods of bleaching required when subunits carrying different fluorophores are studied sequentially increases the risk for errors due to movement of particles into or out of the field of view during the experiment. We chose to address these risks by developing tools for simultaneous, two-color studies. First, we established a two-laser TIRFM strategy to assess both subunits in complexes formed by colocalized E1–TFP and Q1–RFP. This combination of FPs was selected to minimize spectral overlap, allowing independent and concurrent visualization and bleaching of the subunits while avoiding the confounding effects of resonance energy transfer between fluorophores (FRET).

Analysis of simultaneous photobleaching data for colocalized E1–TFP and Q1–RFP demonstrated that complexes were composed of two E1 and four Q1 subunits (Fig. 3*A* and *SI Appendix*, Table S3). Thus, E1–TFP bleaching of 46 particles revealed 91% with two stepwise decreases in fluorescence and 9% with one step, whereas concurrent Q1–RFP bleaching of the same particles showed fractional magnitudes for four, three, two, and one steps of 36%, 44%, 17%, and 2%, respectively (Fig. 3 *B* and *C*). Estimated statistical confidence that the fluorescent particles contained two E1 and four Q1 was >0.999 and 0.99, respectively (*SI Appendix*, Table S3), by the approach of Hines (34).

To perform this analysis, it was necessary first to identify particles that included both E1–TFP and Q1–RFP. This identification was achieved on a pixel-by-pixel basis by using unbiased intensity correlation analysis (*Materials and Methods*) to generate a mean Manders' coefficient of colocalization (33). In this set of experiments, the subunits were expressed at equal levels, and the mean Manders' coefficient was 0.93 ± 0.01 with a particle density of 617×10^{-3} per μm^2, whereas surface particles with only E1–TFP or Q1–RFP were present at just 51×10^{-3} and 42×10^{-3} per μm^2, respectively ($n = 5$ cells) (Fig. 3*D* and *SI Appendix*, Table S4).

Simultaneous, Two-Color, Pore-Toxin-Directed, Single-Particle Photobleaching. Another approach we applied to count the number of E1 subunits in single I_{Ks} channels was to use a fluorophore-bearing toxin that only binds to channels correctly assembled with four α-subunits. This strategy was used to confirm that E1–TFP was colocalized at the cell surface with intact channels and also offered the advantage that channels were identified by a single bleaching step (the fluorophore on the toxin) rather than by up to four steps as required to count Q1 subunits. Again, a 2:4 ratio of E1 to Q1 subunits in I_{Ks} channel complexes was determined (Fig. 4 and *SI Appendix*, Table S3).

Here, we used a Q1 subunit variant (Q1*) that we had previously produced via pore mutation to be sensitive to CTX (19)

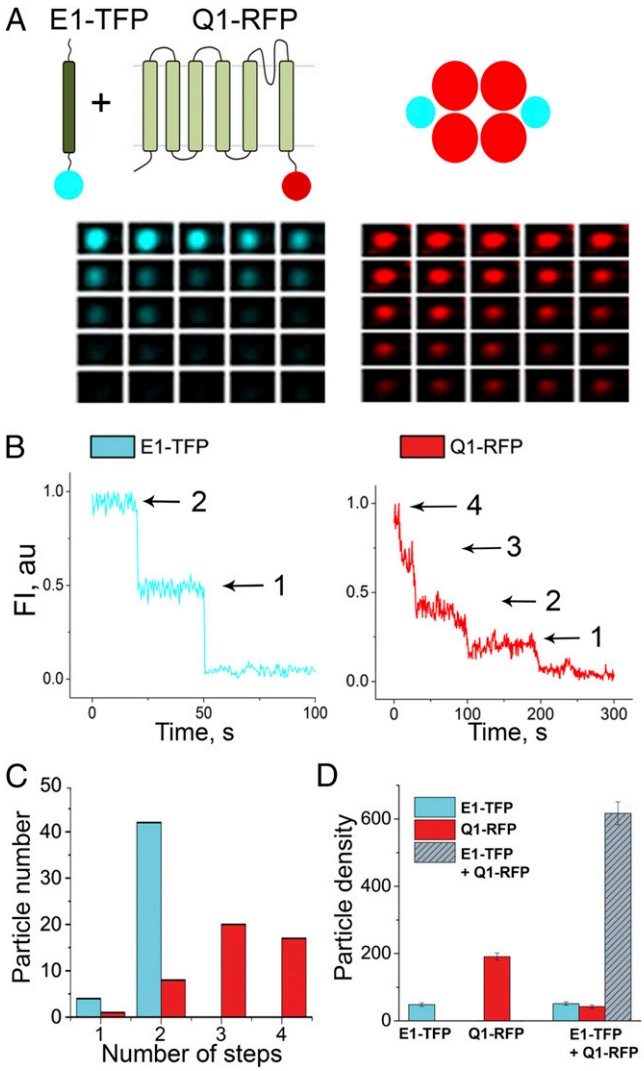

Fig. 3. Simultaneous photobleaching of E1–TFP and Q1–RFP confirms a 2:4 stoichiometry for I_{Ks} channel complexes. Q1–RFP and E1–TFP were studied at the surface of CHO cells by TIRFM and simultaneous single-particle photobleaching. Analysis of bleaching is in *SI Appendix*, Table S3, and analysis of colocalization and surface density is in *SI Appendix*, Table S4. (*A*, *Upper*) Cartoon of Q1–RFP and E1–TFP subunits showing the FPs on the subunit C termini and the subunit stoichiometry determined by this strategy (*SI Appendix*, Table S3). (*Lower*) Montages showing simultaneous photobleaching time courses of TFP (*Left*; teal) and RFP (*Right*; red) in the same, representative single fluorescent particle. Every fifth frame is shown. (*B*) Time courses for simultaneous photobleaching of both fluorophores in the particle in *A*. E1–TFP was bleached in two steps, and Q1–RFP was bleached in four steps (arrows). (*C*) Histogram of photobleaching steps of both E1–TFP (teal bars) and coexpressed Q1–RFP (red bars) studied in the same fluorescent spots. No colocalized particles were observed to bleach with more than two steps for E1–TFP or four steps for Q1–RFP (*SI Appendix*, Table S3). (*D*) Surface-density histogram for subunits based on bleaching steps in cells (using Manders' coefficient of colocalization; *SI Appendix*, Table S4) expressing E1–TFP alone (E1–TFP; teal bar), Q1–RFP alone (Q1–RFP; red bar), or the two subunits expressed together (E1–TFP + Q1–RFP); in the last case, subunits are differentiated if separate (teal or red) or colocalized (striped bar). The surface density of I_{Ks} channels is seen to be ~15 times that for Q1 channels in the same cells (*SI Appendix*, Table S4).

that also binds AgTx2 labeled with a fluorescent dye (tetramethylrhodamine methyl ester; AgTx2–TMRM) on a cysteine that tolerates modifications without loss of binding affinity (Fig. 4*A*) (46, 47). Because one toxin molecule binds to a site in the pore on the central axis of pseudosymmetry, stable interaction requires that all four α-subunits be present in their normal arrangement (1). When Q1* and E1–TFP were coexpressed, the resulting I_{Ks} currents showed biophysical parameters like wild-type channels (*SI Appendix*, Table S1). Furthermore, AgTx2–TMRM suppressed the current in a reversible fashion (Fig. 4*A*), showing a rapid on-rate ($4.5 \pm 0.12\ \mu M^{-1}\cdot s^{-1}$), a slow off-rate ($1.2 \pm 0.05 \times 10^{-3}\ s^{-1}$), a half-maximal equilibrium affinity (K_i)

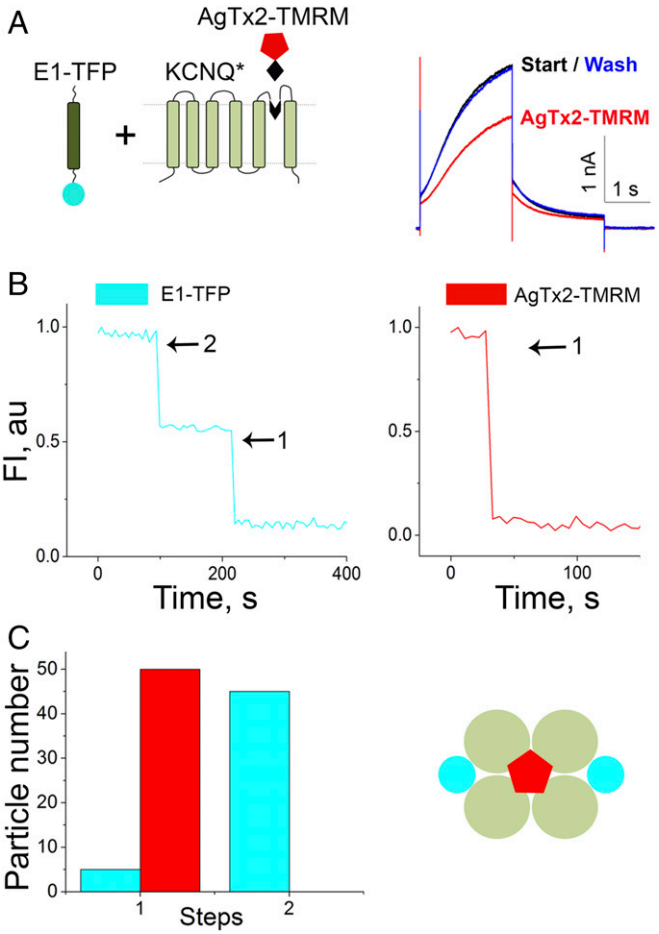

Fig. 4. Simultaneous photobleaching of E1–TFP and AgTx2–TMRM confirm a 2:4 stoichiometry in E1 and Q1* channel complexes. E1–TFP was expressed in CHO cells with Q1*, a variant that binds a single AgTx2–TMRM toxin molecule in the channel pore with a K_i of 280 ± 50 pM (*SI Appendix*, Fig. S1). Q1* + E1–TFP channel currents are like wild-type I_{Ks} channel (*SI Appendix*, Table S1). Simultaneous photobleaching of TFP and TMRM was studied at the surface of CHO cells by TIRFM as in Fig. 3. Analysis of bleaching steps is in *SI Appendix*, Table S3. (*A*, *Left*) Cartoon representation of the Q1*-AgTx2–TMRM, E1–TFP, and Q1* showing the position of the fluorophores on the toxin and E1 C terminus. (*Right*) Block of E1–TFP + Q1* channel currents in a representative CHO cell by 50 pM AgTx2–TMRM with pulses to 60 mV. Currents were evoked every 15 s by 2-s test pulses from a holding potential of −80 mV. The three traces show the start current (black), the current after 180-s exposure to AgTx2–TMRM (red), and recovery of the current 240 s after the toxin is washed away (blue). (*B*) Time courses for simultaneous photobleaching of both fluorophores in a representative fluorescent particle. E1–TFP shows two bleaching steps (*Left*), and AgTx2–TMRM shows a single stepwise decrease in fluorescence intensity (*Right*). (*C*, *Left*) Histogram of bleaching steps for E1–TFP (teal bars) and AgTx2–TMRM (red bar) studied in the same fluorescent spots. No colocalized particles were observed with more than two E1–TFP bleaching steps or one TMRM bleaching step. (*Right*) Cartoon of subunit stoichiometry determined by the strategy (*SI Appendix*, Table S3).

of 280 ± 50 pM, and meeting expectations for a simple, bimolecular interaction (*SI Appendix*, Fig. S1 and Table S3).

Surface particles labeled with AgTx2–TMRM contained E1–TFP with a mean Manders' coefficient of 0.98 ± 0.01 (*SI Appendix*, Table S4; $n = 4$ cells). Simultaneous photobleaching revealed that all particles contained only one AgTx2–TMRM, consistent with the known mechanism of inhibition—pore occlusion by a single toxin molecule (48–50). Of 50 particles with colocalized fluorophores that were studied, 90% showed two E1–TFP bleaching steps and 10% showed one, giving an estimated statistical confidence that the channels contained two E1 and one AgTx2–TMRM that was >0.999 (Fig. 4 *B* and *C* and *SI Appendix*, Table S3). Like channels formed by E1–TFP with Q1–RFP, E1–TFP with Q1* produced an I_{Ks} channel surface density of 657×10^{-3} per μm^2, whereas E1–TFP and AgTx2–TMRM were observed alone at 49×10^{-3} and 33×10^{-3} per μm^2, respectively (*SI Appendix*, Table S4).

High and Low Levels of E1 Do Not Alter I_{Ks} Channel Subunit Stoichiometry. The studies described thus far were performed on cells transformed with equal amounts of E1 and Q1 cDNA. It is reasonable to assume, however, that cells in vivo might produce the two subunits at unequal levels at different times in response to normal stimuli or disease; indeed, Q1 transcripts outnumber E1 transcripts by five to one in preparations of human cardiac ventricle (35, 36). We therefore studied cells with up to 10-fold more or 10-fold less E1 relative to Q1.

Increasing the relative amount of cDNA for E1–TFP by 3 or 10 times over that added for Q1–RFP did not alter the subunit stoichiometry determined by simultaneous, two-color photobleaching; again, we determined I_{Ks} channels to carry two E1 subunits with a statistical confidence of >0.999, and no complex was observed to have more than two E1 subunits (*SI Appendix*, Fig. S2 and Table S3). The biophysical parameters of I_{Ks} currents studied in cells expressing high amounts of E1 also remained unchanged compared with cells expressing a 1:1 ratio of the subunit cDNAs (*SI Appendix*, Fig. S2 and Table S1).

Decreasing the relative amount of cDNA for E1–TFP such that it was 10 times less than that for Q1–RFP had a significant impact on the currents—they appeared to be a mixture of fast Q1 channel-type currents and slow I_{Ks} channel-type currents with a $V_{1/2}$ that was midway between that measured for the two channel types (Fig. 5*A* and *SI Appendix*, Table S1). To determine whether these unique currents included contributions from Q1 channels assembled with a single E1 subunit, as hypothesized by others (23, 25, 31, 32), simultaneous, two-color photobleaching was performed on these cells to assess colocalization of fluorophores and subunit densities.

In cells with low levels of E1 relative to Q1, single-particle photobleaching revealed Q1 channels with no incorporated E1 subunits, I_{Ks} channels with two E1 subunits and the number of channels with a single E1 bleaching event expected due to prebleaching of I_{Ks} channels with two E1 subunits (Fig. 5 *B* and *C* and *SI Appendix*, Tables S3 and S4). Thus, of 102 particles with colocalized fluorophores, 91% had two E1–TFP bleaching steps and 9% had one, and all of these particles were assessed to contain two E1 subunits with an estimated statistical confidence of >0.999. The many complexes with only Q1–RFP subunits showed bleaching steps consistent with formation of intact tetramers with the same high statistical confidence (Fig. 5*C* and *SI Appendix*, Table S3).

E1 Subunits and Channel Trafficking. In addition to altering the biophysical properties of whole-cell currents, expressing 10 times less E1–TFP than Q1–RFP decreased colocalization of the two subunits (Fig. 5*D*). Thus, the mean Manders' coefficient was only 0.58 ± 0.3, and the mean density of colocalized particles was less than half (257×10^{-3} per μm^2) of that observed in cells expressing equal levels of the two subunits or excess E1–TFP (Fig. 5 *D* and *E* and *SI Appendix*, Table S4). The relative density of surface particles with Q1–RFP alone was 188×10^{-3} per μm^2, similar to the density observed when Q1 subunits were expressed without E1 (Fig. 3*D*), and the surface density of E1–TFP alone was low (23×10^{-3} per μm^2) (Fig. 5*E* and *SI Appendix*, Table S4; $n = 5$ cells). These findings confirm that a mixture of I_{Ks} channels (with two E1 subunits) and Q1 channels (with no E1 subunits) (Fig. 5*F*) produce the hybrid currents recorded from these cells.

The single-particle colocalization data suggest an underlying mechanism for surface expression of I_{Ks} channels with two E1 subunits and Q1 channels with no E1 subunits that is consistent with prior macroscopic (biochemical) studies of E1 and Q1 subunit trafficking in mammalian cells (20, 35, 51). We show that little E1–TFP is on the CHO cell surface that is not colocalized with Q1, whether E1 is expressed alone or with Q1 (~23×10^{-3} to 51×10^{-3} per μm^2; *SI Appendix*, Table S4). Of note, all particles in cells expressing E1–TFP alone bleached in a single step, indicating that E1 at the surface is monomeric (*SI Appendix*, Table S2). As expected, Q1 channels formed in the absence of E1 subunits reached (or remained) on the surface at just ~1/3 the density of I_{Ks} channel complexes that have E1; this result supports the notion that E1 favors forward trafficking of Q1, although E1 on its own is retained or recovered rapidly from the surface. Finally, the findings reveal that two E1 are able to augment steady-state surface expression of Q1 channels, whereas a single E1 is insufficient.

Discussion

In this article, we describe single-particle photobleaching methods to assess subunit stoichiometry of ion channels on the surface of live mammalian cells and show that human E1 and Q1 subunits form I_{Ks} channels that carry two E1 subunits. Applying this gold-standard method for subunit counting to mammalian cells with multiple spectroscopic approaches—including simultaneous, two-color counting with varying ratios of E1 to Q1 cDNA—we do not observe fluorescent complexes with more than two E1 subunits. Although the conclusion that I_{Ks} channels carry no more than two E1 subunits is directly supported by failure to observe more than two steps and statistical analysis of the accumulated data, the argument that the channels rarely—and perhaps never—reach the surface with just one E1 subunit is more formally empirical.

Thus, using the most powerful approach that we describe in this report, simultaneous, two-color photobleaching, ~90% of single I_{Ks} channels showed two E1 bleaching steps when E1 and Q1 were coexpressed at equal levels (*SI Appendix*, Table S3). Moreover, ~90% of I_{Ks} channels also showed two E1 bleaching steps when levels of the accessory subunit were 10-fold higher than Q1 subunits and when the channels were formed with E1 and Q1* at equimolar levels and AgTx2-TMRM was used to identify individual channels (*SI Appendix*, Table S3). These findings, and our failure to observe three or four E1 subunits in complexes, establish with high statistical significance, per Hines (34), that I_{Ks} channels carry two E1 subunits, and not more.

One E1 bleaching step was observed in ~10% of I_{Ks} channel complexes with different ratios of the expressed subunits (*SI Appendix*, Tables S3 and S4), as expected if all I_{Ks} channels carry two E1 subunits (based on fluorphore prebleaching and missed events). This result does not exclude the notion that some small fraction of I_{Ks} channels can escape to the cell surface with one E1 subunit. Thus, to our knowledge, no rigorous statistical method has been developed, including that of Hines (34), to quantify the confidence that such lower-order complexes are absent. Nonetheless, strong evidence that channels do not form with one E1 subunit is provided by our studies with limiting levels of E1 subunits that produced hybrid currents (Fig. 5*A*): The spectroscopic data showed a mixture of rapidly activating Q1 channels (with no E1

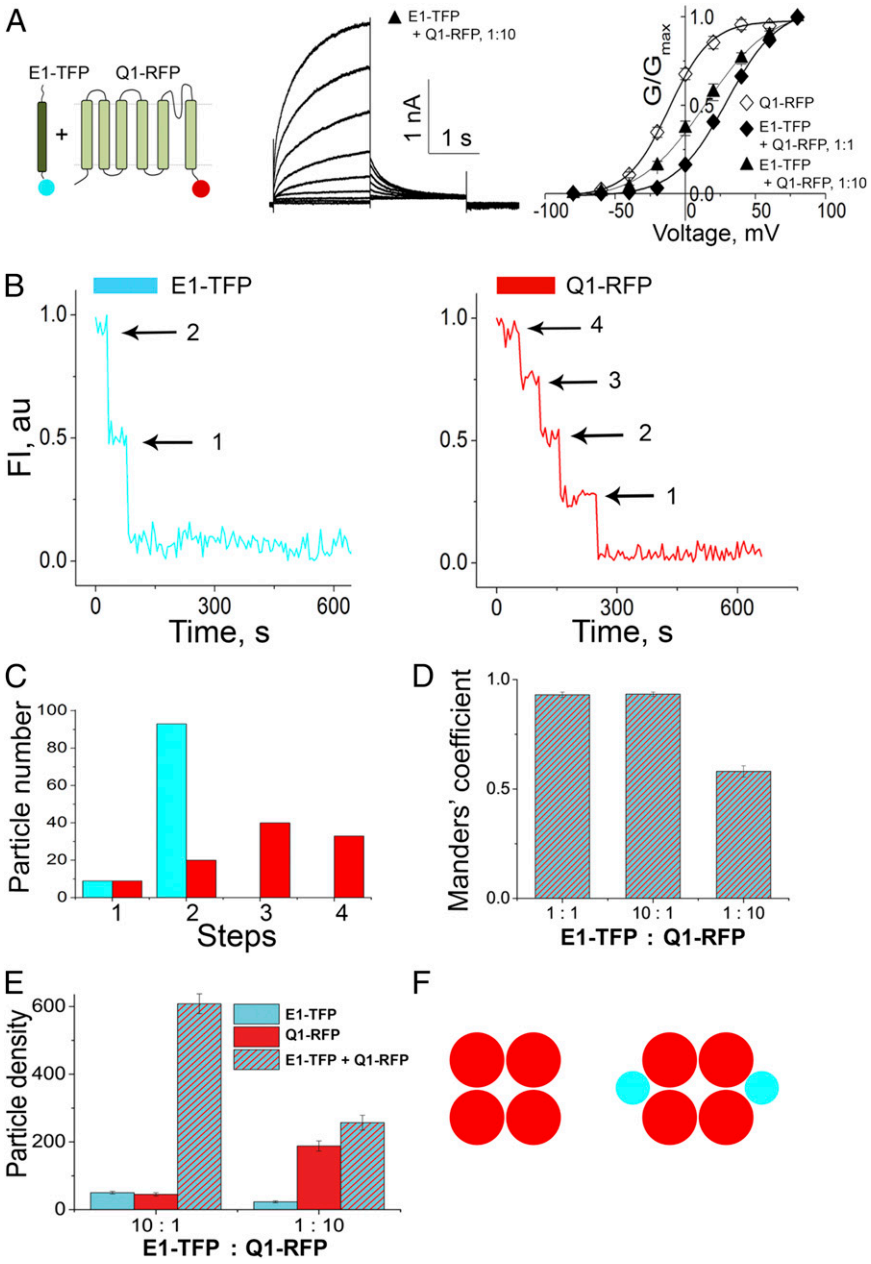

Fig. 5. Limiting amounts of E1–TFP reveal two channel types, those with two E1 subunits and those with none. E1–TFP was added at 1/10th the concentration of Q1–RFP and CHO cells studied by voltage-clamp in whole-cell mode or by TIRFM with simultaneous photobleaching of each FP. Currents were evoked and analyzed as described in *Materials and Methods*. Data are means ± SEM for five cells studied in each group. Biophysical parameters are summarized in *SI Appendix*, Table S1, and the analysis of bleaching steps is in *SI Appendix*, Table S3. (*A*, *Left*) Cartoon of E1–TFP and Q1–RFP showing the FPs on the subunit C termini. (*Center*) Family of whole cell-currents from cells with 10-fold less E1–TFP than Q1–RFP showing a rapid rise in current not seen when E1 + Q1 subunits are expressed at equal levels (Fig. 1*A*). (*Right*) Normalized *G*–*V* relationships for cells expressing Q1–RFP alone (open diamond), equal E1–TFP and Q1–RFP cDNA (1:1; filled diamond), and 10-fold less E1–TFP with Q1–RFP (1:10; filled triangle). (*B*) Time courses for simultaneous photobleaching of both fluorophores in a representative fluorescent particle with E1–TFP and Q1–RFP. E1–TFP bleaches in two steps, and Q1–RFP bleaches in four steps (arrows). (*C*) Histogram of photobleaching steps for E1–TFP (teal bars) and Q1–RFP (red bars) studied in the same fluorescent spots. No colocalized particles were observed to bleach with more than two steps for E1–TFP or four steps for Q1–RFP. (*D*) Histograms of Manders' coefficient of colocalization from cells expressing E1–TFP with Q1–RFP at 1:1, 10:1, or 1:10 ratios (*SI Appendix*, Table S4) showing that ∼half the particles have both E1 and Q1 subunits and half have only Q1 subunits with E1 at 1/10th the level of Q1. (*E*) Surface-density histogram for subunits based on bleaching steps (using Manders' coefficient of colocalization; *SI Appendix*, Table S4) for cells expressing E1–TFP with Q1–RFP at 10:1 and 1:10 ratios showing E1–TFP alone (teal bars), Q1–RFP alone (red bars), or the two subunits when colocalized (striped bar). (*F*) Cartoon representation of the two channel types found on the cell surface when E1 is limiting—Q1 channels with no E1 and I_{Ks} channels with two E1 subunits.

subunits) and slowly activating I_{Ks} channels bearing two E1 subunits (Fig. 5*C*). Thus, when levels of E1 were 10-fold less than Q1, over 40% of channels carried only Q1 subunits, and ∼90% of those channels that did form with E1 subunits showed two E1 bleaching steps, that is, there was no increase in single E1 bleaching events compared to any other subunit expression ratio (*SI Appendix*, Tables S3 and S4). These findings directly refute the hypothesis that hybrid currents result from I_{Ks} channels with

variable numbers of E1 subunits (23, 32). We conclude that channel assembly with two E1 subunits is preferred or, perhaps, is required for steady-state surface expression of I_{Ks} channels.

We suggest that Nakajo et al. (25) concluded in error that the number of E1 subunits in I_{Ks} channels is variable, ranging from one to four E1 subunits per channel, even though they used single-particle photobleaching due to experimental limitations. To minimize mobility of fluorescent particles in oocytes, Nakajo et al. studied subunits that were tagged not only with FPs but also with the PDZ-binding motif from $K_V1.4$ channels and additionally overexpressed the postsynaptic tethering protein PSD-95, thereby risking nonnative, PDZ-mediated subunit aggregations. These manipulations led ~38% of the aggregates with E1 to be sufficiently immobile on the oocyte surface, so they were judged suitable for subunit counting. Further, when using two fluorophores, Nakajo et al. used sequential (asynchronous) bleaching so that challenges due to particle mobility were compounded by an extended duration of photobleaching, risking movement of subunits into and out of the field of view during study. These challenges were not an issue here because I_{Ks} channels and Q1 channels are stable on the CHO cell surface at room temperature [whereas at 37 °C increased membrane fluidity allows study of channel movement (52)], precluding the need for appending subunits with trafficking tags. Moreover, problems studying I_{Ks} channels in oocytes due to the presence of endogenous KCNE and KCNQ subunits are well known (16, 37–39) and resolved by expression in CHO cells (11). Indeed, heterologous expression of other mammalian ion channels in oocytes has been shown to alter subunit stoichiometry (53, 54) and subunit composition (55, 56).

The single-particle surface-density results (*SI Appendix*, Table S4) confirm and extend prior studies that argue for a collaborative role of E1 and Q1 subunits in trafficking. The results support our prior predication that that the increase in macroscopic current seen when Q1 was expressed with E1 was due to an approximately fourfold increase in unitary conductance and an approximately threefold increase in channel surface density (11). Thus, Q1 channel density was $\sim 190 \times 10^{-3}$ per μm^2, and I_{Ks} channel density was $\sim 600 \times 10^{-3}$ per μm^2 whether channels were formed in cells with equal amounts of Q1 and E1 or a 10-fold excess of E1. That E1–TFP is observed at the CHO cell surface at low levels in the absence of Q1 supports biochemical studies showing that the majority of E1 subunits are retained in the ER or *cis*-Golgi in the absence of expressed Q1 and that E1 requires assembly with Q1 or other K_V α-subunits to traffic efficiently to the cell surface (51). The data are also consistent with the conclusion that E1 influences I_{Ks} channel surface levels via control over the rate of internalization (35). Given that cells with a 10-fold excess of Q1 relative to E1 have a Q1 channel density of $\sim 188 \times 10^{-3}$ per μm^2, like that observed in cells with Q1 alone, I_{Ks} channels (with two E1 subunits) at a density of only $\sim 257 \times 10^{-3}$ per μm^2 and few Q1 or E1 subunits on the surface outside of channels, the following biosynthetic mechanism is suggested: E1 goes to the surface poorly on its own or is rapidly recycled; channels with one E1 do not form, suppress forward trafficking, or are rapidly recycled; and channels with two E1 subunits favor surface expression due to enhanced forward trafficking or longer residence on the surface. In keeping with a dimer of dimer model for assembly of α-subunit tetramers (57), assembly of two trimeric assemblies containing two Q1 subunits and one E1 subunit might be operative.

The single-particle photobleaching strategies we describe here to study I_{Ks} channels on the surface of live mammalian cells, particularly via simultaneous, two-color subunit counting combined with assessment of fluorophore colocalization to allow determination of the surface density of assemblies of defined subunit composition, should also prove powerful for consideration of other membrane protein complexes.

MinK, MiRP1, MiRP2, MiRP3, and MiRP4 (E1–E5) have all been shown to assemble with Q1 subunits when heterologously expressed in experimental cells, and all are present in human heart with the potential to assemble with Q1 in vivo (58). MinK is also known to assemble with other K_v channel α-subunits including cardiac HERG (59). Moreover, more than one type of MiRP can be present in a single channel complex (60). We suspect that all these channel complexes (in the heart and elsewhere in the body) will have the same valence—that is, two E-type subunits, no more and no less, and four α-subunits. It is less clear that the same trafficking effects should be assumed. Other channels that incorporate E-type subunits appear to merit the type of scrutiny applied here to I_{Ks} and Q1 channels. Also of interest are questions implied by 2:4 stoichiometry and, we presume, twofold symmetry of the resultant channels; thus, we recently demonstrated that E1 slows the gating kinetics of I_{Ks} channels by slowing the movement of Q1 voltage-sensors (15), but we do not yet know whether all four sensors respond similarly to changes in transmembrane potential or, for example, they manifest two behaviors.

Lack of consensus on the number of E1 subunits in I_{Ks} channels has led to models of cardiac function, models of I_{Ks} channel structure and activity, drug screens for cardiac medications, and the creation of transgenic animals based on the notion that I_{Ks} channels can form with numbers of E1 subunits that we argue are not present in nature. Our findings lead us to conclude that models that incorporate one, three, or four E1 subunits do not reflect I_{Ks} channels on the surface of mammalian cells.

Materials and Methods

Cell Culture, Heterologous Expression, and Encoded Fluorescence Tags. CHO-K1 cells (ATCC no. CCL-61) were maintained in F12K medium with 10% (vol/vol) FBS and 1% penicillin and streptomycin. Wild-type human Q1 [National Center for Biotechnology Information (NCBI) accession no. NM_000218], KCNQ1-ΔS290-V293-E294G-K318I-V319Y-Q321V (Q1*) (19), and wild-type human E1 (NCBI accession no. NP_000210.2) were handled in pRAT, an in-house vector (15). TagRFP-T (RFP), Venus (VFP), and mTFP1 (TFP) genes were inserted in-frame with the C terminus of E1, Q1 and Q1* as described for other FPs (28). Plasmids carrying Q1 or E1 variants were used at a concentration of 1 μg per 1 mL of OptiMEM and were transfected into cells with Lipofectamine 2000 according to the manufacturer's instructions (Life Technologies). To study a 3:1 ratio of E1 to Q1, 3 μg of E1–TFP cDNA was transfected with 1 μg of Q1–RFP cDNA. This mass of cDNA was adjusted to 1 μg of E1–TFP per 0.1 μg of Q1–RFP cDNA to study a 10:1 ratio and 0.1 μg of E1–TFP per 1 μg of Q1–RFP to study a 0.1:1 ratio. All experiments were performed 24–48 h after transfection at room temperature.

Electrophysiology. Whole-cell potassium currents were recorded with an Axopatch 200A amplifier (Molecular Devices) from cells bathed in a perfusate comprising, in mM: 130 NaCl, 4 KCl, 1.2 $MgCl_2$, 2 $CaCl_2$, and 10 Hepes; pH was adjusted to 7.4 with NaOH. Electrodes were fabricated from borosilicate glass (Clark) and had resistances of 2–4 MΩ when filled with a solution containing, in mM: 130 KCl, 1 $MgCl_2$, 5 EGTA, 5 K_2ATP, and 10 Hepes; pH was adjusted to 7.4 with KOH. Cells had a mean whole-cell capacitance of 13 ± 0.56 pF; series resistance was typically ~5 MΩ, and the voltage-error of <3 mV was not adjusted for. Cells for study were selected based on fluorescence color. Cells expressing subunits without FP tags were identified by using cotransfected EGFP. Currents were evoked with 2-s test pulses from −80 to 80 mV from a holding potential of −80 mV, with 20-mV increments. Tail currents were recorded at −40 mV for 2 s. The interpulse interval was 15 s. Conductance (G) was calculated from the tail currents and expressed as G/G_{max} as a function of the membrane voltage. G–V curves were obtained as before (15) and were fit to the equation

$$G = Gmax \Big/ \left[1 + \exp\left(-zF\left(V - V\tfrac{1}{2}\right)\Big/RT\right)\right],$$

where V is the test potential, $V_{1/2}$ is the voltage of half-maximal activation, z is the effective valence, T is the temperature, R is the gas constant, and F is the Faraday constant. Activation and deactivation kinetics were analyzed by fitting the current traces with a single-exponential equation and are reported as τ_{act} and τ_{deact}, respectively. Block of Q1* + E1 channels by AgTx2 was studied by applying dilutions of AgTx2-N5C (C S Bio), labeled with TMRM (Life Technologies) in the presence of 0.1% BSA. The K_{on}, K_{off}, and K_i

values of the interaction were calculated as described (19). All electrophysiological data were analyzed in pClamp (Molecular Devices), Excel, and OriginLab software.

Single-Particle Photobleaching. Single protein complexes at the surface of live CHO cells were identified by using TIRFM as described (28). The critical angle for TIRF was adjusted by using a CellTIRF illuminator (Olympus) and a high-numerical-aperture apochromat objective (150x, 1.45 NA; Olympus) mounted on an automated fluorescence microscope (IX81; Olympus) controlled by Metamorph software (Molecular Devices). For simultaneous illumination of two fluorophores, CellTIRF software (Olympus) was used to adjust the critical angle for each excitation wavelength to generate evanescent waves of equivalent depth (100 nm). RFP and TMRM (Life Technologies) were excited by a 561-nm laser line, and VFP and TFP were excited by 515- and 445-nm laser lines, respectively. When TFP was studied with either RFP or TMRM, emitted light signals were split by using a 520-nm dichroic mirror mounted in a DualView adapter (Photometrics), and each wavelength was directed to one-half of a back-illuminated EM-CCD (Hammamatsu). The DualView dichroic mirror was disengaged when single fluorophores were studied.

Analysis of Fluorescence Colocalization and Subunit Stoichiometry. Fluorophores were photobleached by continual excitation, and data were captured as movies of 100–400 frames acquired at 1 Hz. When TFP was studied with RFP or AgTx2–TMRM in the same cell, the data for each fluorophore were saved as separate stacks and processed in an identical manner. Misalignment of the data between stacks was corrected in ImageJ by using the StackReg plugin. Next, the degree of colocalization between two fluorophores was determined by unbiased intensity correlation analysis using the Coloc2 plugin to obtain the Manders' coefficient for each cell. For stoichiometric analysis, fluorescent spots were defined as a discrete 3 × 3-pixel region around a pixel of maximum intensity, as described (27, 28, 41). Fluorescence is reported as the change in fluorescence normalized by the initial level of fluorescence for each trace. Statistical analyses to assess the estimated confidence with which stoichiometry could be inferred from the observed data and θ, the probability of successfully observing each possible photobleaching event, were performed in R Studio, according to methods developed by Hines (34). It is notable that all three FPs studied showed high θ values when appended to E1, and, further, that mTFP1 had a high θ value appended to E1 in multiple experimental contexts. The densities of colocalized and single fluor-fluorescent spots were determined following thresholding and watershed separation in ImageJ. Then, the particle number was counted in four separate 30 by 30-pixel regions of interest for five cells per group by using the Analyze particles plugin.

Labeling AgTx2 with TMRM. Synthetic Agitoxin2-N5C (C S Bio) was incubated with TMRM (Life Technologies) at room temperature at a ratio of 1:1 and purified by HPLC using a gradient of 10–40% acetonitrile over 45 min.

ACKNOWLEDGMENTS. We thank K. J. Ruscic for insightful discussion; E. Dowdell and R. Agafonov for technical support; R. Y. Tsien (University of California San Diego) for TagRFP-T; and A. Periasamy (University of Virginia) for mVenus and mTFP1 fluorescence tags. The work was supported by National Institutes of Health Grant R01HL105959 (to S.A.N.G.).

1. MacKinnon R (1991) Determination of the subunit stoichiometry of a voltage-activated potassium channel. *Nature* 350(6315):232–235.
2. Doyle DA, et al. (1998) The structure of the potassium channel: Molecular basis of K^+ conduction and selectivity. *Science* 280(5360):69–77.
3. Jiang YX, et al. (2003) X-ray structure of a voltage-dependent K^+ channel. *Nature* 423(6935):33–41.
4. Abbott GW, Goldstein SAN (1998) A superfamily of small potassium channel subunits: Form and function of the MinK-related peptides (MiRPs). *Q Rev Biophys* 31(4): 357–398.
5. Abbott GW, et al. (1999) MiRP1 forms IKr potassium channels with HERG and is associated with cardiac arrhythmia. *Cell* 97(2):175–187.
6. Abbott GW, et al. (2001) MiRP2 forms potassium channels in skeletal muscle with Kv3.4 and is associated with periodic paralysis. *Cell* 104(2):217–231.
7. Abbott GW, Goldstein SAN (2001) Potassium channel subunits encoded by the *KCNE* gene family: Physiology and pathophysiology of the MinK-related peptides (MiRPs). *Mol Interv* 1(2):95–107.
8. McCrossan ZA, Abbott GW (2004) The MinK-related peptides. *Neuropharmacology* 47(6):787–821.
9. Tai KK, Goldstein SAN (1998) The conduction pore of a cardiac potassium channel. *Nature* 391(6667):605–608.
10. Goldstein SA, Miller C (1991) Site-specific mutations in a minimal voltage-dependent K^+ channel alter ion selectivity and open-channel block. *Neuron* 7(3):403–408.
11. Sesti F, Goldstein SAN (1998) Single-channel characteristics of wild-type I_{Ks} channels and channels formed with two minK mutants that cause long QT syndrome. *J Gen Physiol* 112(6):651–663.
12. Yang Y, Sigworth FJ (1998) Single-channel properties of IKs potassium channels. *J Gen Physiol* 112(6):665–678.
13. Cai S-Q, Hernandez L, Wang Y, Park KH, Sesti F (2005) MPS-1 is a K+ channel beta-subunit and a serine/threonine kinase. *Nat Neurosci* 8(11):1503–1509.
14. Sesti F, et al. (2000) A common polymorphism associated with antibiotic-induced cardiac arrhythmia. *Proc Natl Acad Sci USA* 97(19):10613–10618.
15. Ruscic KJ, et al. (2013) IKs channels open slowly because KCNE1 accessory subunits slow the movement of S4 voltage sensors in KCNQ1 pore-forming subunits. *Proc Natl Acad Sci USA* 110(7):E559–E566.
16. Sanguinetti MC, et al. (1996) Coassembly of K(V)LQT1 and minK (IsK) proteins to form cardiac $I(_{Ks})$ potassium channel. *Nature* 384(6604):80–83.
17. Barhanin J, et al. (1996) K(V)LQT1 and IsK (minK) proteins associate to form the I(Ks) cardiac potassium current. *Nature* 384(6604):78–80.
18. Wang KW, Goldstein SAN (1995) Subunit composition of minK potassium channels. *Neuron* 14(6):1303–1309.
19. Chen H, Kim LA, Rajan S, Xu S, Goldstein SAN (2003) Charybdotoxin binding in the $I(_{Ks})$ pore demonstrates two MinK subunits in each channel complex. *Neuron* 40(1): 15–23.
20. Morin TJ, Kobertz WR (2008) Counting membrane-embedded KCNE beta-subunits in functioning K+ channel complexes. *Proc Natl Acad Sci USA* 105(5):1478–1482.
21. Tzounopoulos T, Guy HR, Durell S, Adelman JP, Maylie J (1995) min K channels form by assembly of at least 14 subunits. *Proc Natl Acad Sci USA* 92(21):9593–9597.
22. Wang W, Xia J, Kass RS (1998) MinK-KvLQT1 fusion proteins, evidence for multiple stoichiometries of the assembled IsK channel. *J Biol Chem* 273(51):34069–34074.
23. Wang K, et al. (2011) Biophysical properties of slow potassium channels in human embryonic stem cell derived cardiomyocytes implicate subunit stoichiometry. *J Physiol* 589(Pt 24):6093–6104.
24. Wang M, Kass RS (2012) Stoichiometry of the slow I(ks) potassium channel in human embryonic stem cell-derived myocytes. *Pediatr Cardiol* 33(6):938–942.
25. Nakajo K, Ulbrich MH, Kubo Y, Isacoff EY (2010) Stoichiometry of the KCNQ1 - KCNE1 ion channel complex. *Proc Natl Acad Sci USA* 107(44):18862–18867.
26. Tombola F, Ulbrich MH, Isacoff EY (2008) The voltage-gated proton channel Hv1 has two pores, each controlled by one voltage sensor. *Neuron* 58(4):546–556.
27. Plant LD, et al. (2010) One SUMO is sufficient to silence the dimeric potassium channel K2P1. *Proc Natl Acad Sci USA* 107(23):10743–10748.
28. Plant LD, Dowdell EJ, Dementieva IS, Marks JD, Goldstein SAN (2011) SUMO modification of cell surface Kv2.1 potassium channels regulates the activity of rat hippocampal neurons. *J Gen Physiol* 137(5):441–454.
29. Sakmann B, Neher E, eds (1995) *Single-Channel Recording* (Plenum, New York), 2nd Ed.
30. Li Y, Chen L, Kass RS, Dessauer CW (2012) The A-kinase anchoring protein Yotiao facilitates complex formation between adenylyl cyclase type 9 and the IKs potassium channel in heart. *J Biol Chem* 287(35):29815–29824.
31. Osteen JD, Sampson KJ, Kass RS (2010) The cardiac IKs channel, complex indeed. *Proc Natl Acad Sci USA* 107(44):18751–18752.
32. Yu H, et al. (2013) Dynamic subunit stoichiometry confers a progressive continuum of pharmacological sensitivity by KCNQ potassium channels. *Proc Natl Acad Sci USA* 110(21):8732–8737.
33. Manders EMM, Verbeek FJ, Aten JA (1993) Measurement of co-localization of objects in dual-colour confocal images. *J Microsc* 169(3):375–382.
34. Hines KE (2013) Inferring subunit stoichiometry from single molecule photobleaching. *J Gen Physiol* 141(6):737–746.
35. Xu X, et al. (2009) MinK-dependent internalization of the IKs potassium channel. *Cardiovasc Res* 82(3):430–438.
36. Gaborit N, et al. (2007) Regional and tissue specific transcript signatures of ion channel genes in the non-diseased human heart. *J Physiol* 582(Pt 2):675–693.
37. Tai K-K, Wang K-W, Goldstein SAN (1997) MinK potassium channels are heteromultimeric complexes. *J Biol Chem* 272(3):1654–1658.
38. Anantharam A, et al. (2003) RNA interference reveals that endogenous *Xenopus* MinK-related peptides govern mammalian K^+ channel function in oocyte expression studies. *J Biol Chem* 278(14):11739–11745.
39. Gordon E, Roepke TK, Abbott GW (2006) Endogenous KCNE subunits govern Kv2.1 K+ channel activation kinetics in Xenopus oocyte studies. *Biophys J* 90(4):1223–1231.
40. Leake MC, et al. (2006) Stoichiometry and turnover in single, functioning membrane protein complexes. *Nature* 443(7109):355–358.
41. Ulbrich MH, Isacoff EY (2007) Subunit counting in membrane-bound proteins. *Nat Methods* 4(4):319–321.
42. Kohout SC, Ulbrich MH, Bell SC, Isacoff EY (2008) Subunit organization and functional transitions in Ci-VSP. *Nat Struct Mol Biol* 15(1):106–108.
43. Plant LD, Zuniga L, Araki D, Marks JD, Goldstein SA (2012) SUMOylation silences heterodimeric TASK potassium channels containing K2P1 subunits in cerebellar granule neurons. *Sci Signal* 5(251):ra84.
44. Fox PD, Loftus RJ, Tamkun MM (2013) Regulation of Kv2.1 K(+) conductance by cell surface channel density. *J Neurosci* 33(3):1259–1270.
45. McGuire H, Aurousseau MR, Bowie D, Blunck R (2012) Automating single subunit counting of membrane proteins in mammalian cells. *J Biol Chem* 287(43):35912–35921.
46. Shimony E, Sun T, Kolmakova-Partensky L, Miller C (1994) Engineering a uniquely reactive thiol into a cysteine-rich peptide. *Protein Eng* 7(4):503–507.

47. Posson DJ, Ge P, Miller C, Bezanilla F, Selvin PR (2005) Small vertical movement of a K+ channel voltage sensor measured with luminescence energy transfer. *Nature* 436(7052): 848–851.
48. MacKinnon R, Miller C (1988) Mechanism of charybdotoxin block of the high-conductance, Ca^{2+}-activated K^+ channel. *J Gen Physiol* 91(3):335–349.
49. Goldstein SA, Miller C (1993) Mechanism of charybdotoxin block of a voltage-gated K^+ channel. *Biophys J* 65(4):1613–1619.
50. Banerjee A, Lee A, Campbell E, MacKinnon R (2013) Structure of a pore-blocking toxin in complex with a eukaryotic voltage-dependent K(+) channel. *eLife* 2:e00594.
51. Chandrasekhar KD, Bas T, Kobertz WR (2006) KCNE1 subunits require co-assembly with K+ channels for efficient trafficking and cell surface expression. *J Biol Chem* 281(52):40015–40023.
52. Mashanov GI, Nobles M, Harmer SC, Molloy JE, Tinker A (2010) Direct observation of individual KCNQ1 potassium channels reveals their distinctive diffusive behavior. *J Biol Chem* 285(6):3664–3675.
53. Sivilotti LG, et al. (1997) Recombinant nicotinic receptors, expressed in Xenopus oocytes, do not resemble native rat sympathetic ganglion receptors in single-channel behaviour. *J Physiol* 500(Pt 1):123–138.
54. Krashia P, et al. (2010) Human $\alpha3\beta4$ neuronal nicotinic receptors show different stoichiometry if they are expressed in Xenopus oocytes or mammalian HEK293 cells. *PLoS ONE* 5(10):e13611.
55. Schmidt C, Hollmann M (2008) Apparent homomeric NR1 currents observed in Xenopus oocytes are caused by an endogenous NR2 subunit. *J Mol Biol* 376(3): 658–670.
56. Buller AL, White MM (1990) Functional acetylcholine receptors expressed in Xenopus oocytes after injection of Torpedo beta, gamma, and delta subunit RNAs are a consequence of endogenous oocyte gene expression. *Mol Pharmacol* 37(3):423–428.
57. Tu L, Deutsch C (1999) Evidence for dimerization of dimers in K^+ channel assembly. *Biophys J* 76(4):2004–2017.
58. Lundquist AL, et al. (2005) Expression of multiple KCNE genes in human heart may enable variable modulation of $I_{(Ks)}$. *J Mol Cell Cardiol* 38(2):277–287.
59. McDonald TV, et al. (1997) A minK-HERG complex regulates the cardiac potassium current I(Kr). *Nature* 388(6639):289–292.
60. Morin TJ, Kobertz WR (2007) A derivatized scorpion toxin reveals the functional output of heteromeric KCNQ1-KCNE K+ channel complexes. *ACS Chem Biol* 2(7): 469–473.